Optoelectronic modeling of perovskite solar cells using TMM and SCAPS-1D

Zh. B. Omarova[1], A. K. Dossymbekova [1], A.M. Yessentay [1] *, D. Y. Yerezhep [1,2]*

[1] Satbayev University, Almaty, 050013, Kazakhstan, darhan_13@physics.kz.
[2] Almaty Management University, Almaty, 050060, Kazakhstan

INTRODUCTION

The increasing demand for clean energy has driven rapid progress in perovskite solar cells (PSCs), whose power conversion efficiency (PCE) has risen from 3.8% in 2009 [1] to over 26.9% today [2]. PSCs offer advantages such as low-cost solution processing, tunable optoelectronic properties, and compatibility with flexible substrates [3].

However, commercialization remains limited by poor long-term stability and lead toxicity concerns [4–6]. To address these challenges, two key material strategies have emerged:

(i) All-inorganic perovskites (e.g., CsPbI3), which provide improved thermal stability and suitable band gaps (~1.73 eV), and

(ii) Mixed cation–mixed halide systems (e.g., $FA_{0.75}Cs_{0.25}Pb(I_{0.8}Br_{0.2})_3$), which enhance phase stability and enable band gap tuning for tandem applications [Science, DOI links].

Optimizing these materials requires accurate modeling. The transfer matrix method (TMM) enables precise optical analysis of multilayer structures, capturing interference effects and improving photogeneration predictions compared to Beer–Lambert models [7]. At the device level, SCAPS-1D simulations solve charge transport equations to evaluate photovoltaic performance and guide parameter optimization [8].

Despite their individual strengths, integrated TMM–SCAPS modeling approaches remain limited [9, 10]. In this work, we combine both methods to simulate planar n–i–p PSCs with CsPbI3 and Cs25Br20 absorbers in an FTO/TiO2/Perovskite/Spiro-OMeTAD/Au structure. This approach enables self-consistent optoelectronic analysis and reveals how material properties influence device performance.

Our results provide optimized device parameters and highlight key differences between all-inorganic and mixed perovskites, offering practical insights for next-generation high-efficiency solar cells.

MATERIALS AND METHODS

In this work, perovskite solar cells (PSCs) are used with the following architecture: ITO/TiO_2/perovskite/Spiro-OMeTAD, as schematically shown in Figure 1.

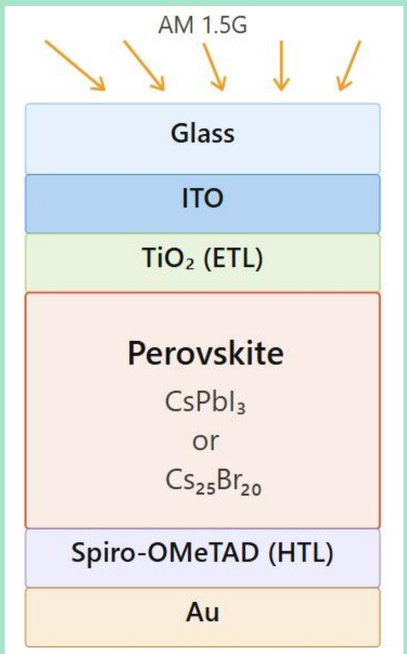

Fig. 1. Schematic representation of the structure of the simulated devices

The optical simulation of the multilayer PSC structure was performed using the transfer matrix method (TMM), implemented in TMM-Sim 1.2 [11]. The TMM−Sim software is written in Python 3 and employs four Python libraries: Pandas [12], NumPy [13], SciPy [14] and Matplotlib [15]. The method has been widely adopted for optical design of perovskite-based photovoltaic devices due to its computational efficiency and ability to account for thin-film interference effects [16].

The electrical simulation was performed using the one-dimensional Solar Cell Capacitance Simulator (SCAPS-1D, version 3.3.10), developed at the University of Gent [17]. SCAPS-1D self-consistently solves the coupled system of the Poisson equation and the drift-diffusion continuity equations for electrons and holes under steady-state illumination:

$$\frac{\partial n}{\partial t} + \frac{\partial J_n}{\partial x} - G_n + R_{\text{net}} = 0 \quad (1)$$

$$\frac{\partial p}{\partial t} + \frac{\partial J_p}{\partial x} - G_p + R_{\text{net}} = 0 \quad (2)$$

$$\varepsilon_m(x)\frac{\partial}{\partial x}\left(\frac{\partial \psi}{\partial x}\right) = \frac{q}{\varepsilon_0}\left[n - p + N_A^- - N_D^+ - \frac{\rho_{\text{def}}}{q}\right] \quad (3)$$

where n and p are the free electron and hole densities; J_n and J_p are the corresponding current densities; G is the generation rate; R_{net} is the net recombination rate; ε_0 and ε_m are the vacuum and material permittivities; ψ is the electrostatic potential; N_A^- and N_D^+ are ionized acceptor and donor densities; and ρ_{def} is the defect charge density.

RESULTS AND DISCUSSION

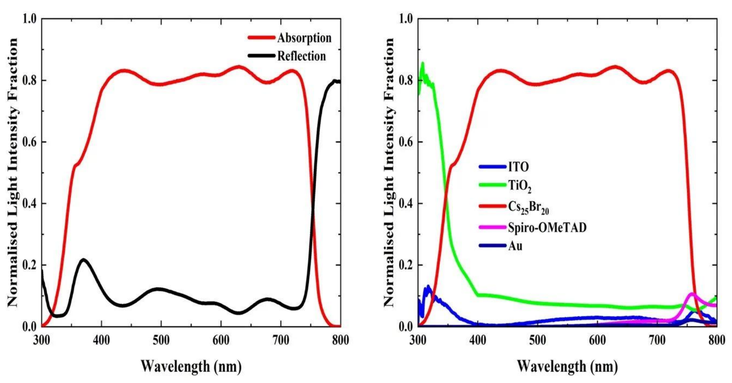

Fig. 2. Normalised light intensity fraction of (a) the absorption and reflection of ITO/TiO_2/perovskite/Spiro-OMeTAD/Au, and (b) absorption in ITO, TiO_2, $CsPbI_3$ and $Cs_{25}Br_{20}$, Spiro-OMeTAD, and Au of the complete PV structure.

The optical characteristics of the ITO/TiO_2/$Cs_{25}Br_{20}$/Spiro-OMeTAD/Au structure were calculated using the transfer matrix method (TMM) (Fig. 2). The total absorption of the device reaches ~80–85% in the 400–750 nm range, while the reflectance does not exceed ~10–13% in the visible region. Layer-by-layer analysis (Fig. 2, right) shows that the majority of photons are absorbed by the active $Cs_{25}Br_{20}$ layer, while parasitic losses in ITO and TiO_2 are concentrated in the UV region (300–380 nm), and the contribution of Spiro-OMeTAD and Au is insignificant and manifests itself primarily near the absorption edge (>700 nm).

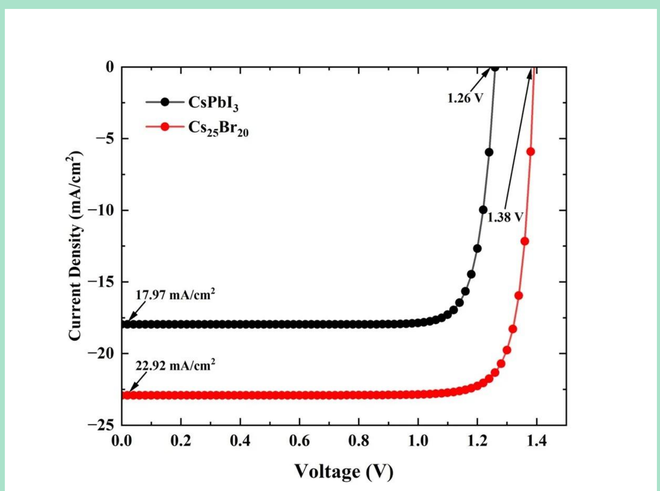

Fig. 3. Current density vs Voltage (J-V) characteristics.

Figure 3 shows the J–V curves for two perovskite absorbers. The $CsPbI_3$-based device exhibits J_{SC} = 17.97 mA/cm² and V_{OC} = 1.26 V, while the $Cs_{25}Br_{20}$ structure exhibits significantly higher values: J_{SC}= 22.92 mA/cm² and V_{OC} = 1.38 V. The increase in V_{OC} is due to optimized energy band alignment in the $Cs_{25}Br_{20}$ structure, and the increase in J_sc is due to improved optical absorption and more efficient charge carrier collection.

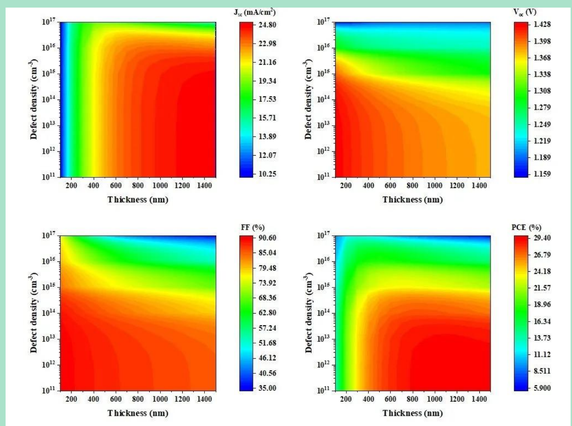

Fig. 4. Impacts of thickness and defect density on output metrics of the designed PSC.

Two-dimensional maps of J_{SC}, V_{OC}, *FF*, and *PCE* as functions of absorber thickness (200–1500 nm) and defect density (10^{11}–10^{17} cm^{-3}) are shown in Fig. 4. The maximum PCE ≈ 29.4% is achieved at a thickness of ~600–800 nm and a defect density ≤10^{13} cm^{-3}. J_{SC} increases with increasing thickness, reaching a plateau (~24.8 mA/cm²) at ≥800 nm. V_{OC} is most sensitive to the defect density: at $N_t > 10^{15}$ cm^{-3}, a sharp drop to ~1.16 V is observed. FF maintains high values (>85%) over a wide range of thicknesses at low defect density but degrades with a simultaneous increase in thickness and N_t due to increased recombination.

CONCLUSIONS

This study included comprehensive multiscale modeling of perovskite solar cells based on $CsPbI_3$ and $Cs_{25}Br_{20}$ with an ITO/ TiO_2/perovskite/Spiro-OMeTAD/Au architecture using the TMM and SCAPS-1D methods. Optical modeling revealed that the main parasitic losses are concentrated in the UV region and are due to absorption in ITO and TiO_2, while the active layer effectively absorbs ~80–85% of incident radiation in the visible range. A comparative analysis of the two compositions revealed the advantage of $Cs_{25}Br_{20}$, which provides a simultaneous increase in both the JSC (22.92 vs. 17.97 мА/см²) and V_{OC} (1.38 vs. 1.26 V). Parametric optimization identified optimal conditions for achieving a PCE of ≈29.4%: an absorber thickness of 600–800 nm and a defect density of ≤10^{13} см$^{-3}$. A comparison of the EQE spectra calculated using the SCAPS-1D and TMM methods confirmed the need for a combined use of electrical and optical modeling to adequately describe the device's photovoltaic characteristics. The obtained results can serve as a guide for the experimental optimization of all-inorganic perovskite solar cells.

REFERENCES

[1] A. Kojima, K. Teshima, Y. Shirai, T. Miyasaka, Organometal halide perovskites as visible-light sensitizers for photovoltaic cells, J. Am. Chem. Soc. 131 (2009) 6050–6051. **DOI:** https://doi.org/10.1021/ja809598r

[2] M.A. Green, E.D. Dunlop, M. Yoshita, N. Kopidakis, K. Bothe, G. Siefer, X. Hao, J. Jiang, Solar cell efficiency tables (version 67), Prog. Photovolt. Res. Appl. 34 (2026) 482–496. **DOI:** https://doi.org/10.1002/pip.70068

[3] H.J. Snaith, Perovskites: The emergence of a new era for low-cost, high-efficiency solar cells, J. Phys. Chem. Lett. 4 (2013) 3623–3630. **DOI:** https://doi.org/10.1021/jz4020162

[4] N.-G. Park, K. Zhu, Scalable fabrication and coating methods for perovskite solar cells and solar modules, Nat. Rev. Mater. 5 (2020) 333–350. **DOI:** https://doi.org/10.1038/s41578-019-0176-2

[5] F. Hao, C.C. Stoumpos, D.H. Cao, R.P.H. Chang, M.G. Kanatzidis, Lead-free solid-state organic–inorganic halide perovskite solar cells, Nat. Photonics 8 (2014) 489–494. **DOI:** https://doi.org/10.1038/nphoton.2014.82

[6] A.H. Slavney, T. Hu, A.M. Lindenberg, H.I. Karunadasa, A bismuth-halide double perovskite with long carrier recombination lifetime for photovoltaic applications, J. Am. Chem. Soc. 138 (2016) 2138–2141. **DOI:** https://doi.org/10.1021/jacs.5b13294

[7] L.A.A. Pettersson, L.S. Roman, O. Inganäs, Modeling photocurrent action spectra of photovoltaic devices based on organic thin films, J. Appl. Phys. 86 (1999) 487–496. **DOI:** https://doi.org/10.1063/1.370757

[8] M. Burgelman, P. Nollet, S. Degrave, Modelling polycrystalline semiconductor solar cells, Thin Solid Films 361–362 (2000) 527–532. **DOI:** https://doi.org/10.1016/S0040-6090(99)00825-1

[9] T. Bendib, L. Bencherif, M.A. Abdi, F. Meddour, Combined optical-electrical modeling of perovskite solar cell with an optimized design, Opt. Mater. 109 (2020) 110259. **DOI:** https://doi.org/10.1016/j.optmat.2020.110259

[10] Bojar, Aleksandra, et al. "Optical simulations and optimization of perovskite/CI (G) S tandem solar cells using the transfer matrix method." *Journal of Physics: Energy* 5.3 (2023): 035001. https://doi.org/10.1088/2515-7655/acec34

[11] Benatto L, Mesquita O, Pacheco KRM, Roman LS, Koehler M, Capaz RB, et al. TMM−Sim: A versatile tool for optical simulation of thin−film solar cells. Comput Phys Commun 2024;300:109206. https://doi.org/10.1016/j.cpc.2024.109206

[12] McKinney W. Data Structures for Statistical Computing in Python, 2010, p. 56–61. https://doi.org/10.25080/Majora-92bf1922-00a

[13] Harris CR, Millman KJ, van der Walt SJ, Gommers R, Virtanen P, Cournapeau D, et al. Array programming with NumPy. Nature 2020;585:357–62. https://doi.org/10.1038/s41586-020-2649-2

[14] Virtanen P, Gommers R, Oliphant TE, Haberland M, Reddy T, Cournapeau D, et al. SciPy 1.0: fundamental algorithms for scientific computing in Python. Nat Methods 2020;17:261–72. https://doi.org/10.1038/s41592-019-0686-2

[15] Hunter JD. Matplotlib: A 2D Graphics Environment. Comput Sci Eng 2007;9:90–5. https://doi.org/10.1109/MCSE.2007.55

[16] Sachchidanand, Kumar A, Sharma P. Transfer matrix method-based efficiency enhancement of lead-free Cs3Sb2Br9 perovskite solar cell. Sol Energy 2023;259:63–71. https://doi.org/10.1016/j.solener.2023.05.014

[17] Burgelman M, Nollet P, Degrave S. Modelling polycrystalline semiconductor solar cells. Thin Solid Films 2000;361–362:527–32. https://doi.org/10.1016/S0040-6090(99)00825-1